Mapping the G-Actin Binding Surface of Cofilin Using Synchrotron Protein Footprinting†

Jing-Qu Guan,‡,§ Sergeui Vorobiev,|| Steven C. Almo,‡,|| and Mark R. Chance*,‡,§,||

Center for Synchrotron Biosciences, Department of Physiology and Biophysics, and Department of Biochemistry, Albert Einstein College of Medicine, 1300 Morris Park Avenue, Bronx, New York 10461

Received December 3, 2001; Revised Manuscript Received February 5, 2002

ABSTRACT: Cofilin is an actin regulatory protein that binds to both monomeric and filamentous actin, and has filament severing activity. Although crystal structures for the monomeric forms of both G-actin and cofilin have been described, the structure of the binary cofilin−G-actin complex is not available. Synchrotron protein footprinting is used to identify specific side chain residues on the cofilin surface that are buried in the formation of the cofilin−G-actin binary complex. Exposure to synchrotron X-rays results in stable oxidative modifications of aromatic, aliphatic, and sulfur-containing side chains, with the rate of modification for a particular residue being dependent on its intrinsic reactivity and solvent accessibility. The rates of modification were monitored for a number of peptides generated by digestion of oxidized cofilin, both in isolation and in its binary complex with G-actin. After binding to G-actin takes place, a significant decrease in modification rates, indicating protection of side chain groups, is seen for cofilin peptides corresponding to residues 4−20, 10−17, 83−96, 91−105, and 106−117. A number of other peptides show no change in reactivity, and are presumed to represent regions distal to the binding site. Tandem mass spectrometry demonstrates that residues Leu 13, Pro 94, Met 99, and Leu 108 and 112 directly participate in the binding interface. These results are generally consistent with, and complementary to, the results of previous site-directed mutagenesis studies and extend our understanding of the G-actin binding surface of cofilin.

Dynamic remodeling of the actin cytoskeleton is essential to cell locomotion, cytokinesis, and complex morphogenetic and developmental programs in multicellular organisms, and pathological states such as neoplastic transformation and tumor metastasis (*1*−*8*). All of these processes involve the site specific assembly and disassembly of filamentous actin networks in response to intracellular and extracellular signals. As the association and dissociation of actin monomers occur exclusively at filament ends, a number of mechanisms have evolved that govern the efficient generation, utilization, and subcellular localization of filament ends.

Cofilin severs actin filaments by disrupting the noncovalent interactions between adjacent actin monomers, resulting in the formation of new filament ends that contribute to both assembly and disassembly. Cofilin binds to both G-actin[1] and F-actin, and severs filaments in a pH-dependent manner (*9*−*14*). The severing activity generates new free barbed ends, which can result in increased rates of depolymerization if the concentration of G-actin is below the critical concentration for polymerization (∼0.1 μM). Alternatively, if the concentration of G-actin is above the critical concentration, severing will result in increased rates of polymerization (*15*). It has also been suggested that cofilin can enhance depolymerization by increasing the off-rate from the pointed end and sequestering G-actin in an unpolymerizable heterodimer (*10*, *16*−*20*). The actin-associated activities of cofilin are inhibited by the LIM-kinase-catalyzed phosphorylation of a serine residue located near the N-terminus (*21*−*23*). The interactions with actin can also be inhibited by phosphoinositides such as PIP_2 (*24*), a property shared with other actin-associated proteins such as gelsolin, villin, and profilin (*25*).

The interactions between cofilin and G- and F-actin have been investigated by various approaches. Electron cryomicroscopy studies of the human cofilin−platelet F-actin complex have shown that cofilin contacts two actin subunits in the filament, one at the cleft between subdomains 1 and 3 of the "upper" subunit and the other on the interface formed by subdomains 1 and 2 of the "lower" subunit (*26*, *27*). Mutagenesis and biochemical studies have identified residues that are essential for both G- and F-actin binding, and residues that contribute specifically to F-actin binding (*28*−

† This work is supported through the Innovative Molecular Analysis Technologies Program of the National Cancer Institute (Grant R33-CA-84173), the NIH Biomedical Technology Program of the Division of Research Resources (Grant P41-RR01633), and NIH Grant R01-GM-53807. The National Synchrotron Light Source at Brookhaven National Laboratory is supported by the Department of Energy, Division of Materials Sciences.

* To whom correspondence should be addressed: Department of Physiology and Biophysics, Albert Einstein College of Medicine, 1300 Morris Park Ave., Bronx, NY 10461. Phone: (718) 430-4136. Fax: (718) 430-8587. E-mail: mrc@aecom.yu.edu.

‡ Center for Synchrotron Biosciences.

§ Department of Physiology and Biophysics.

|| Department of Biochemistry.

[1] Abbreviations: G-actin, monomeric actin; F-actin, filamentous actin; DTT, dithiothreitol; PAGE, polyacrylamide gel electrophoresis; PIP_2, phosphatidylinositol 3,4-diphosphate; TFA, trifluoroacetic acid; HPLC, high-performance liquid chromatography; MS, mass spectrometry; ESI, electrospray ionization; MALDI-TOF, matrix-assisted laser desorption ionization time-of-flight.

10.1021/bi0121104 CCC: $22.00
Published on Web 04/16/2002

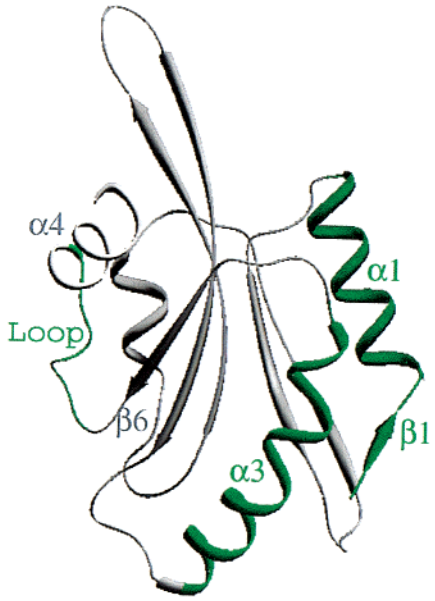

FIGURE 1: Crystal structure of yeast cofilin (*46*). Mutagenesis and cross-linking studies suggest that the G-actin binding surface of cofilin (colored green) includes the N-terminus (α1 and *β*1), the long helix α3, and the loop connecting strands *β*6 and α4. This figure was prepared with SETOR (*55*).

31). Cross-linking experiments also implicate the N-terminus as a site of interaction with actin (*32*). Overall, the studies indicate that the G-actin binding surface of cofilin includes the N-terminus (helix α1 and strand *β*1), the long central α3 helix, and the loop connecting strand *β*6 and helix α4 (Figure 1). In the case of the F-actin binding surface, additional contributions from *β*6 and α4 are indicated. On the basis of the structural homology between cofilin and gelsolin segment 1, modeling and computational studies have suggested that cofilin binds to the cleft formed by subdomains 1 and 3 in G-actin, as observed for gelsolin segment 1 (*33*, *34*).

Protein footprinting using synchrotron radiation relies on hydroxyl radicals produced through radiolysis of water to modify solvent accessible side chains on the surfaces of proteins. We have previously shown that millisecond exposure to a synchrotron white beam produces substantial oxidation of accessible residues in both peptides and proteins and that the rate of modification is positively correlated with the solvent accessibility of the modified residues (*35*−*37*). Thus, the reactive residues can serve as markers for changes in solvent accessibility (*36*−*38*). The residues most susceptible to oxidation and, those that are the most useful probes, are the sulfur-containing and aromatic residues, in addition to proline and leucine (*35*). The final oxidation products of hydroxyl radical attack under the conditions of synchrotron protein footprinting are generally stable and well-understood based on established oxidative mechanisms from radiation chemistry (*36*, *37*, *39*, *40*). The overall technique is illustrated in Figure 2. The oxidized samples are generated by X-ray exposure in the first step. To assay the rates and sites of modification, we have used specific proteolytic digestion of the oxidized proteins and mass spectrometry of the individual peptides. Typical oxidations of accessible side chains result in a mass shift of 16*n*, where *n* is the number of oxygen atoms incorporated into the reactive side chain groups. Since the proteolytic digestions are designed to provide a unique mass product, the peptides that undergo oxidation are easily distinguished from those that are resistant. Tandem mass spectrometry and collision-induced dissociation (*41*, *42*) can be used to unambiguously identify the specific site of modification (*35*−*38*, *43*−*45*). Such specific identification of incorporation sites has also been successfully used in deuterium exchange studies of protein structure (*43*, *44*). In this investigation, tandem MS was successful in uniquely identifying the cofilin side chains that become specifically protected from modification as a consequence of their participation in the binary cofilin−G-actin complex.

The crystal structures of both G-actin and cofilin have been reported (*46*−*48*) so that potentially reactive and accessible side chain residues of the monomers can be predicted. However, the atomic structure of the cofilin−actin complex remains unknown. In this paper, we use synchrotron protein footprinting to probe the actin binding surface of cofilin using an approach similar to that used previously for probing the actin binding surface of gelsolin segment 1 (*45*). Our results here show a significant decrease in the modification rate for cofilin peptides including residues 4−20 and 83−96 (generated from a trypsin digest) and peptides including residues 10−17, 91−105, and 106−117 (generated from an Asp-N digest), while all other observed peptides exhibit no significant changes in the modification rate. Tandem MS was used to identify the reactive residues within these peptides; overall, we find that residues Leu 13, Pro 94, Met 99, and Leu 108 and 112 are protected upon formation of the complex. We also demonstrated that the modification rates of Leu 21, at the end of α1, as well as Leu 32 were unaffected by complex formation, suggesting that these residues do not directly contribute to the binding site. Overall, our footprinting results are consistent with previous biochemical and genetic studies and allow a clearer definition of the actin binding surface of cofilin.

EXPERIMENTAL PROCEDURES

Preparation of Proteins. Rabbit skeleton actin was prepared by the method of Spudich and Watt (*49*) and further purified by gel filtration. Actin was stored at 4 °C in dialysis against G-buffer [2 mM Tris (pH 8.0), 0.2 mM ATP, 0.5 mM DTT, 0.2 mM $CaCl_2$, and 1 mM NaN_3], which was freshly prepared and exchanged daily.

Yeast cofilin cDNA was subcloned into the pGEX2T vector, and expressed as a glutathione *S*-transferase (GST) fusion protein in *Escherichia coli* JM109 cells, as reported previously (*28*). The GST-bound cofilin was enriched with glutathione−agarose affinity chromatography and cleaved with thrombin and the cofilin purified by gel filtration or a Superdex75 HiLoad column (Pharmacia Biotech) that had been equilibrated with cofilin buffer [10 mM Tris (pH 7.5) and 50 mM NaCl]. Fractions containing cofilin were pooled and frozen at −80 °C. The plasmid sequence was verified by DNA sequencing and the protein identity confirmed by mass spectrometry.

Determination of the Protein Concentrations. Protein concentrations were determined by amino acid analysis at the Biotechnology Resource Laboratory of Yale University (New Haven, CT) (Beckman 7300 Amino Acid Analyzer, postcolumn ninhydrin detection). The error of the duplicate analyses for each protein sample was within 3%.

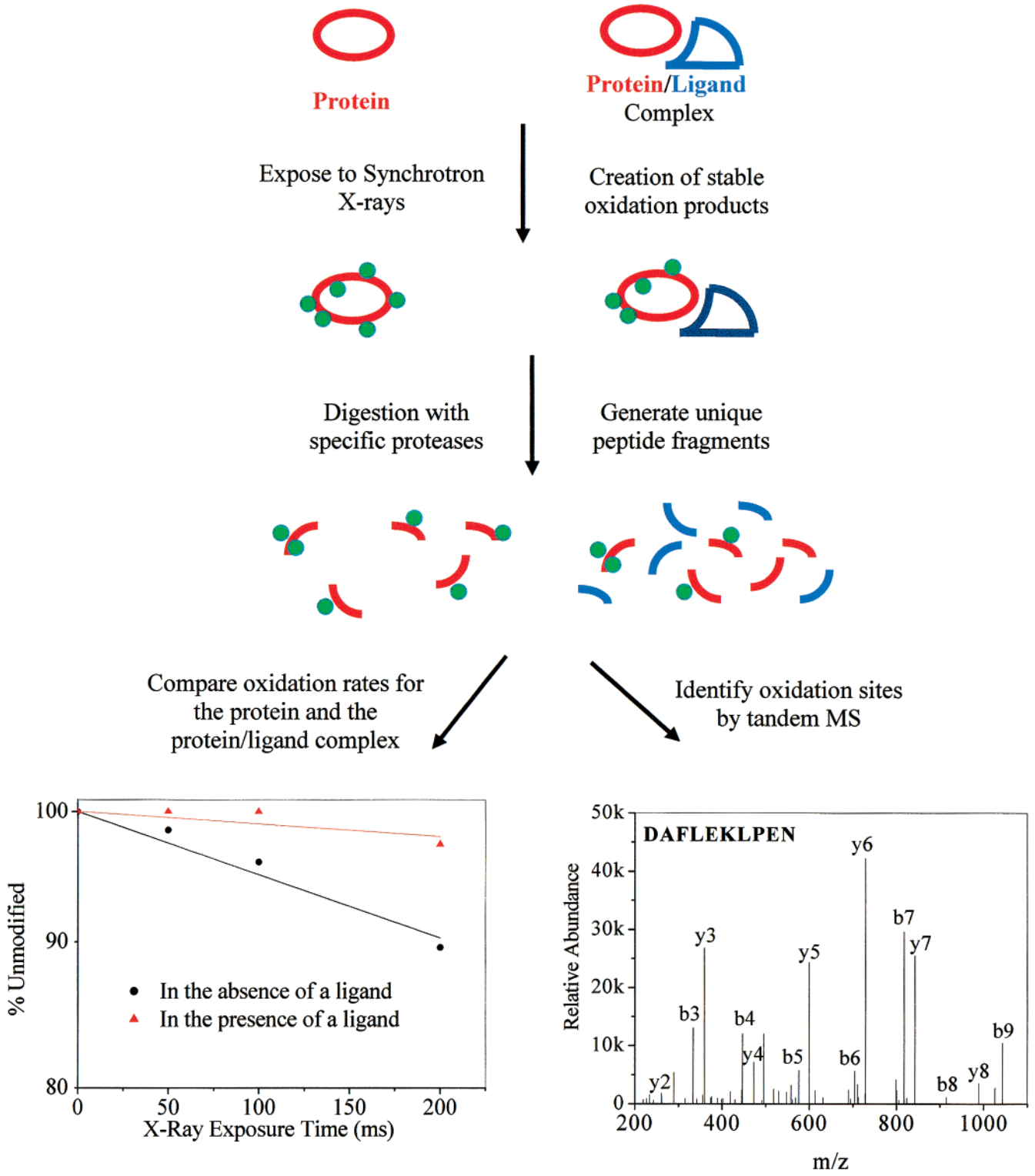

FIGURE 2: Schematic representation of the synchrotron X-ray footprinting technique. A protein and its complex with a ligand are exposed to synchrotron X-rays, which produce hydroxyl radicals that modify side chains of the protein. After this X-ray exposure, the protein samples are digested with proteases, and MS is applied to quantitate the extent of modification. This quantitation provides information about the solvent accessibility of each peptide in both the isolated and complexed states. The particular modification sites are determined by tandem MS (MS/MS). In the dose−response example, a slower rate of modification is seen for the peptide when isolated from the complex than for the free protein. Thus, it is indicated that this peptide contains reactive side chain residues participating in the interface.

Native PAGE Analysis. Formation of the cofilin−G-actin complex was examined using 10 to 20% native acrylamide gels (BioWhittaker Molecular Applications) run at 70 V for 7 h or 100 V for 3 h, in a running buffer containing 25 mM Tris, 193 mM glycine, 0.2 mM ATP, and 0.2 mM $CaCl_2$ (pH 8.0). Gels were stained for 10 h with 0.1% Brilliant Blue R-250 (Fisher Biotech) in 50% MeOH and 10% HOAc, and destained for 7 h in 10% MeOH and 7% HOAc. The gels were analyzed on a Low Light-Imaging System equipped with a digital camera (Alpha Innotech Corp.) and the intensities of the individual bands quantified using ImageQuant 5.0 software (Molecular Dynamics).

Measuring the Dissociation Constant. For determination of the dissociation constant (K_d), the concentration of G-actin was fixed at 1.35 μM, and that of cofilin varied from 0 to 3.4 μM for the native gel analysis. Quantitation of the bands in native gels yielded the relative amount of G-actin, cofilin, and the actin−cofilin complex, which were used to calculate the amounts of bound actin and free cofilin for each titration point. Plotting $(C_0 - C_1)/C_0$ (C_0 is the total concentration of G-actin and C_1 that of free G-actin) versus the concentration of free cofilin produced the titration curve, from which the K_d was derived using Origin 5.0 software (Microcal Software, Inc.). To establish that the native gels and the use of digital imaging analysis produced quantitative results, control experiments were carried out to identify the linear regime for this analysis. In these experiments, defined amounts of protein monomer and preformed complex were run in different lanes and the intensities of the bands measured. It was determined that the protein concentration was linear with respect to band intensity at a complex concentration of <1.6 μM and at an actin or cofilin monomer concentration of <2.5 μM. Thus, we could accurately measure the concentration of the actin monomer, cofilin monomer, and complex in the same gel to accurately determine the free cofilin concentration.

Calculation of Solvent Accessible Area (ASA). The solvent accessible surface areas of all side chains were calculated for the yeast cofilin (PDB entry 1CFY) crystal structure using the program VADAR 1.2 (Canadian Protein Engineering Network, University of Alberta, Edmonton, Canada; the results are shown in Table 1).[2]

Radiolysis. Prior to radiolysis experiments, actin and cofilin were dialyzed against the buffers used in the radiolysis experiments. The actin radiolysis buffer consisted of 2 mM sodium cacodylate (pH 8.0), 0.2 mM $CaCl_2$, and 0.2 mM ATP. The cofilin radiolysis buffer consisted of 20 mM sodium cacodylate (pH 8.0) and 50 mM NaCl. The complex was formed by incubating 10 μM actin and 10 μM cofilin in the above buffers at 4 °C for 2−4 h prior to X-ray exposure. Control radiolysis experiments were performed on cofilin in the G-actin radiolysis buffer, which showed that no protections on cofilin were induced by the introduction of G-actin buffer (data not shown). All synchrotron protein footprinting experiments were performed at the X-28C beamline of the National Synchrotron Light Source (NSLS, Brookhaven National Laboratory, Upton, NY) (*51*). Exposure times were controlled by using an electronic shutter (Vincent Associates) and ranged from 0 to 200 ms. The storage ring energy was 2.8 GeV, and ring currents ranged from 136 to 289 mA throughout all the experiments in this study. The unattenuated X-rays exit the storage ring beampipe through a beryllium window and travel through ~50 cm of air before reaching the sample tube. The samples were stored at −20 °C following X-ray exposure.

Enzymatic Proteolysis. Radiolyzed samples were denatured in acetonitrile prior to proteolysis with sequencing grade modified trypsin (Promeaga) and endoproteinase Asp-N (Roche). The proteases were added in two aliquots to the protein samples, yielding a final weight:weight ratio of 1:40 for trypsin [in 50 mM NH_4HCO_3 (pH 7.8)] and 1:20 for Asp-N [in 25 mM Na_3PO_4 (pH 8.0)]. All samples contained 0.05 M guanidine chloride, and the Asp-N digestion additionally required $CoCl_2$ (1 mM) and 10% acetonitrile. Digestions were performed at 37 °C for 15−17 h. Note that we do not report data on all possible peptides that could be derived from cofilin; in this paper, we report on the peptides that ionized well and gave data with a high signal-to-noise ratio. Thus, our coverage of the protein is not complete.

Table 1: Modification Rates of Cofilin Peptides[a]

Protease	Peptide	Most Likely Modified Amino Acid(s)	Modification Rate (s^{-1})	
			Cofilin	Cofilin-Actin
Trypsin	4-20 (m/z 1735.9) SGVAVADESLTAFNDLK **51 1.4 0.2**	13L	0.54 ± 0.02	0.20 ± 0.09
	27-36 (m/z1137.3) FILFGLNDAK **0.1 7.8 0 1**	32L	0.23 ± 0.03	0.23 ± 0.04
	43-56 (m/z1602.7) ETSTDPSYDAFLEK **90 15 0 32**	48P, 50Y, 53F, 54L	0.53± 0.12	0.41± 0.06
	83-96 (m/z 1634.9) IVFFTWSPDTAPVR **0.4 1.5 1.3 6.4 73**	94P	0.83 ± 0.16	0.20 ± 0.05
AspN	10-17 (m/z 895.4) DESLTAFN **51 1.4**	13L	0.51 ± 0.04	0.10 ± 0.03
	18-33 (m/z1896.1) DLKLGKKYKFILFGLN **0.2 120 34 0.1 7.8 0 1.3**	21L	0.95 ± 0.18	0.92 ± 0.17
	51-60 (m/z 1174.6) DAFLEKLPEN **0 32 0.8 47**	*b*	1.15 ± 0.14	1.05 ± 0.16
	91-105 (m/z 1638.9) DTAPVRSKMVYASSK **73 111 21**	99M	≈ 44	0.39± 0.05
	106-117 (m/z 1271.7) DALRRALNGVST **0 0**	108L, 112L	0.11 ± 0.02	0.02 ± 0.02
	123-129 (m/z 845.3) DFSEVSY **82 95**	124F	0.86 ± 0.06	0.82 ± 0.07
	130-143 (m/z 1468.7) DSVLERVSRGAGSH **96**	133L, 143H	0.91 ± 0.05	0.80 ± 0.12

[a] The modifiable amino acids are in bold, under which the accessible surface area (ASA) values are indicated. Accessible surface areas of reactive amino acid side chains were calculated with VADARA 1.2 software (*50*, *57*), based on the crystal structure of yeast cofilin (*46*). The modified amino acids were identified via MS/MS or are indicated by reactivity and solvent accessibility where MS/MS was not conclusive (see the text). [b] The modified amino acids cannot be accurately determined; for details, see the text.

Peptide Analysis. Reverse phase HPLC was performed on a Waters 2690 Separations Module (Waters Corp.), using a C18 (Vydac) 1.0 mm × 150 mm column for all digested protein samples. Two buffer systems were used to establish a gradient for chromatographic separation. Initially, pure buffer A (95% water, 5% acetonitrile, and 0.06% TFA) is used, which is mixed with buffer B (90% acetonitrile, 10% water, and 0.055% TFA) such that a change in composition of 2% per minute is established. Note that for the digested binary complex, a mixture of actin and cofilin peptides must be separated. The analysis of the actin peptides will be presented in a separate publication.

Electrospray Ionization Mass Spectrometry. Following enzymatic proteolysis, the resulting peptide mixtures were separated and analyzed using a coupled HPLC−ESI-MS LCQ system (ThermoQuest Corp.), with a flow rate of 50 μL/min. The HPLC eluate was directed to a Finigan LCQ quardrupole ion trap mass spectrometer with a needle voltage of 4.5 kV. β-Casomorphin (YPFVEPI) was used for tuning the instrument and setting up instrument methods for peptide analyses. The samples were scanned for 60−75 min, and

[2] Solvent accessible surface areas of reactive amino acid side chains were calculated from the crystal structures of yeast cofilin and G-actin, by using the VADAR computer algorithm (Canadian Protein Engineering Network, University of Alberta).

the spectra were acquired in the positive ion mode for masses corresponding to an *m*/*z* range of 400−2000. The sites of oxidative modification were determined by tandem HPLC−MS/MS sequencing as per our previous publications (*35*−*38*). The peptide mixtures were separated by reverse phase HPLC and the eluates directed to the LCQ ion trap mass spectrometer, under the same conditions described above. For the acquisition of MS/MS data, a 1.0 unit *m*/*z* range was used in selecting the parent ion for fragmentation in the second stage of the mass spectrometer.

MALDI-TOF (Matrix-Assisted Laser Desorption Ionization) Mass Spectrometry. MALDI-TOF mass spectra were acquired on a Voyager DE-STR TOF mass spectrometer (Perseptives Biosystems). A solution of α-cyano-4-hydroxycinammic acid in 50% acetonitrile and 0.1% TFA was used to prepare the matrix for ionization. Samples (1−1.5 μL) containing mixtures with a 1:5 to 1:10 (v:v) protein digest: matrix solution ratio were spotted on a MALDI sample target and air-dried. Spectra were acquired in the linear mode for positive ions using an acceleration voltage of 25 000 V. Approximately 100 scans were averaged for each spectrum.

Modification Rates. Dose responses were obtained from the LCQ spectra of the digested peptide samples. The relative abundance of the modified and unmodified peptide ions was used to calculate the unmodified fraction (the ratio of ion intensity of the unmodified peptide to the sum of ion intensity from the modified and unmodified peptide) as a function of exposure to the synchrotron X-ray beam. Thus, the fraction unmodified used in the dose response (1 − modified/total) is consistently calculated for all exposure times and for both the free protein and cofilin in its binary complex. Throughout all the calculations, the most abundant charge state (usually doubly charged) was used, and the calculation of the modified total includes all observed products (e.g., +16, +32, etc.). If the modifications alter the degree of ionization (due to suppression effects), the reported extent of modification may be off by a constant factor that reflects such differences in ionization efficiency. Yet, such differences will not affect the identification of protected regions. Evidence that digestion conditions or peptide sequence minimally affects the measured rates is provided by comparison of the results from peptides 4−20 (trypsin digest) and 10−17 (Asp-N digest) shown in Table 1. Despite entirely different digestion conditions, identical rates of modification (within the respective errors) are observed for both isolated cofilin and the complex.

Any background modification seen in the unexposed sample is subtracted from the totals; occasionally, some methionine-containing peptides have a background oxidation of a few percent. The abundance for each individual peptide at each time point was normalized to that at zero exposure time, where the fraction unmodified is set to 1.0. The dose−response curves are presented as unmodified fraction (plotted on a logarithmic scale) versus X-ray exposure time and fit as described below. The rate constant data (including standard deviations) are shown in Table 1. The data are the result of three independent experiments. Because of the constant concentration of hydroxyl radicals in the samples during the exposure (*45*, *51*), the modification reactions of analyzed peptides obey first-order kinetics. Thus, the curves were fit to the equation $A = A_0e^{-kt}$, in which A and A_0 are the amount of a peptide at times t and 0, respectively, and k is the modification rate constant (Origin 5.0, Microcal Software, Inc.).

RESULTS

Native PAGE Analysis. The activities of the proteins, as well as conditions for the formation of the actin−cofilin complex, were confirmed by native PAGE analysis. A band distinct from those for both cofilin and actin represents the formation of the complex (Figure 3a). Complex formation saturated when the concentration of free cofilin exceeded 1.35 μM, showing the complex was formed in 1:1 molar ratio (Figure 3b). This stoichiometry is consistent with that reported previously (*52*, *53*). As under some circumstances human cofilin has been suggested to bind to F-actin in a 2:1 molar ratio (*27*), yeast cofilin and G-actin in a molar ratio of 50:1 were also examined by native PAGE, but no additional species were detected (data not shown). These observations show that under the experimental conditions used for footprinting, yeast cofilin forms an equimolar complex with G-actin. The titration yielded a K_d of ∼0.2 μM for the yeast cofilin−rabbit muscle G-actin interaction. As all footprinting experiments were carried out at a cofilin concentration of 10 μM (well above those seen in the native gel), >95% complex formation is assured.

Correlation of the Side Chain Reactivity with the Solvent Accessibility. Synchrotron protein footprinting is sensitive to changes in the solvent accessible surface areas (ASAs) of discrete amino acids as monitored by their relative reactivities to hydroxyl radicals (*37*, *45*). This can be demonstrated when the specific residues that contribute to the peptide's reactivity are identified by tandem MS (see below). For example, in isolated cofilin, the side chain of Leu 21 (120 Å^2) is more than twice as accessible to solvent as that of Leu 13 (51 Å^2). Consistent with this difference in accessibility (Table 1), peptide 18−33 (for which Leu 21 is the predominant oxidized residue) is oxidized at approximately twice the rate of peptide 4−20 or 10−17 (where Leu 13 is the oxidation target). For the peptide comprised of residues 27−36, the modification rate is lower still at 0.23 s^{-1}. Leu 32 (the predominant target) has an accessible surface area of 7.8 Å^2, and its modification rate is much lower than those of both Leu 21 and Leu 13. Though the relationship between accessibility and reactivity is not strictly proportional, the reactivity does decrease monotonically with decreased solvent accessibility as we have shown previously for lysozyme (*37*). Chemically similar side chains have similar reactivities; on the other hand, aromatic and sulfur-containing residues have a higher reactivity to hydroxyl radicals, while others can be refractory to oxidation and react more slowly (e.g., glycine). Our studies to date suggest the following reactivity order: Cys and Met ≫ Phe, Tyr, and Trp > Pro > His and Leu (*36*, *37*).

Dose−Response Curves. Figure 4 shows representative dose−response curves for three cofilin peptides. Peptide 91−105 exhibits the fastest rate of modification in the case of isolated cofilin, ca. 44 s^{-1} (Figure 4a). Within this sequence, there are three amino acids at which modifications are likely to occur (Table 1). Because this peptide contains the highly reactive methionine residue that is entirely accessible (111 Å^2), substantial oxidation occurred on this peptide even at the shortest exposure time of 50 ms. Nevertheless, this rate

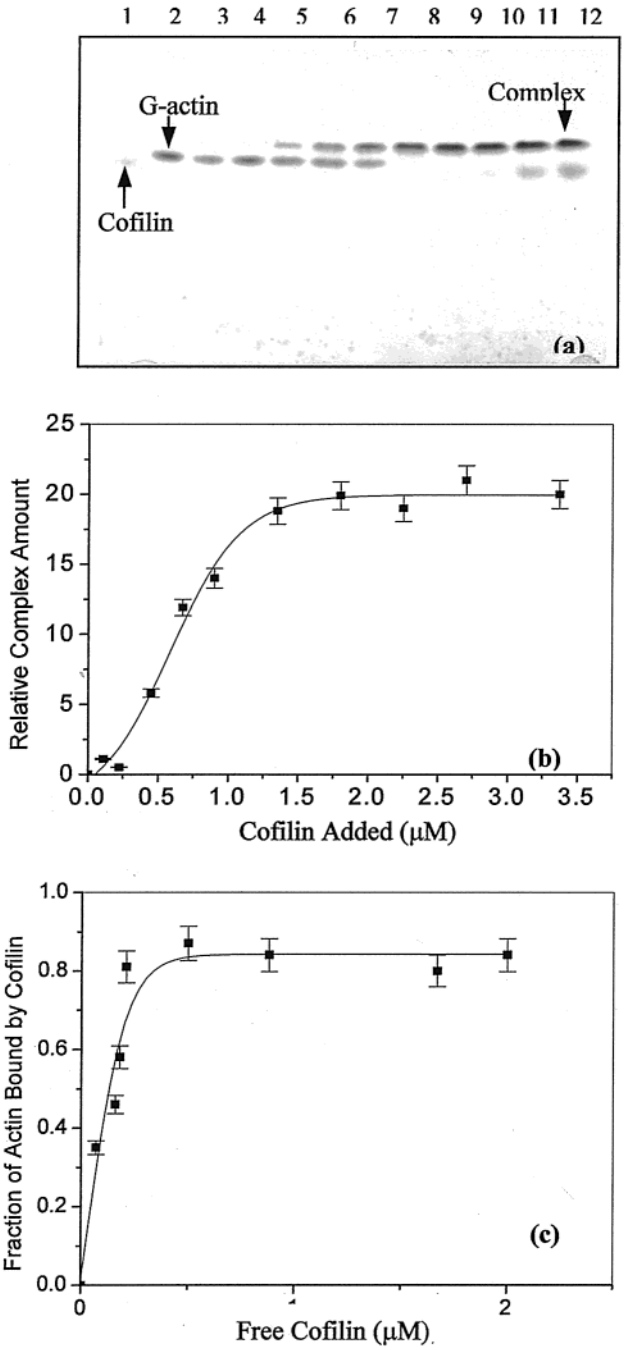

FIGURE 3: Native PAGE analysis. (a) Distinct migration bands for G-actin, cofilin, and the cofilin−G-actin complex indicate the formation of their complex. The gel was run with a running buffer composed of 25 mM Tris, 192 mM glycine, 0.2 mM ATP, and 0.2 mM Ca^{2+} (pH 8.0). The concentration of actin was 1.34 μM, and the concentration of cofilin was 1.35, 0, 0.11, 0.22, 0.45, 0.67, 0.9, 1.35, 1.8, 2.25, 2.7, and 3.4 μM in lanes 1−12, respectively. (b) The amount of cofilin added (*x*-axis) is plotted vs the band intensity of the complex (*y*-axis). The titration curve shows the extent of complex formation peaks when the molar ratio of the binary components reaches 1:1. (c) The free cofilin concentration (*x*-axis) is plotted vs the fraction of actin bound (*y*-axis). A K_d of 0.2 μM was derived from the data.

dramatically decreased to 0.39 s^{-1} when cofilin is bound to G-actin (Figure 4a). Peptide 123−129, however, does not exhibit any oxidation rate variation; the dose−response curve is independent of G-actin binding (Figure 4b). Figure 4c shows the behavior of peptide 83−96, and its reactivity is significantly lower for the complex.

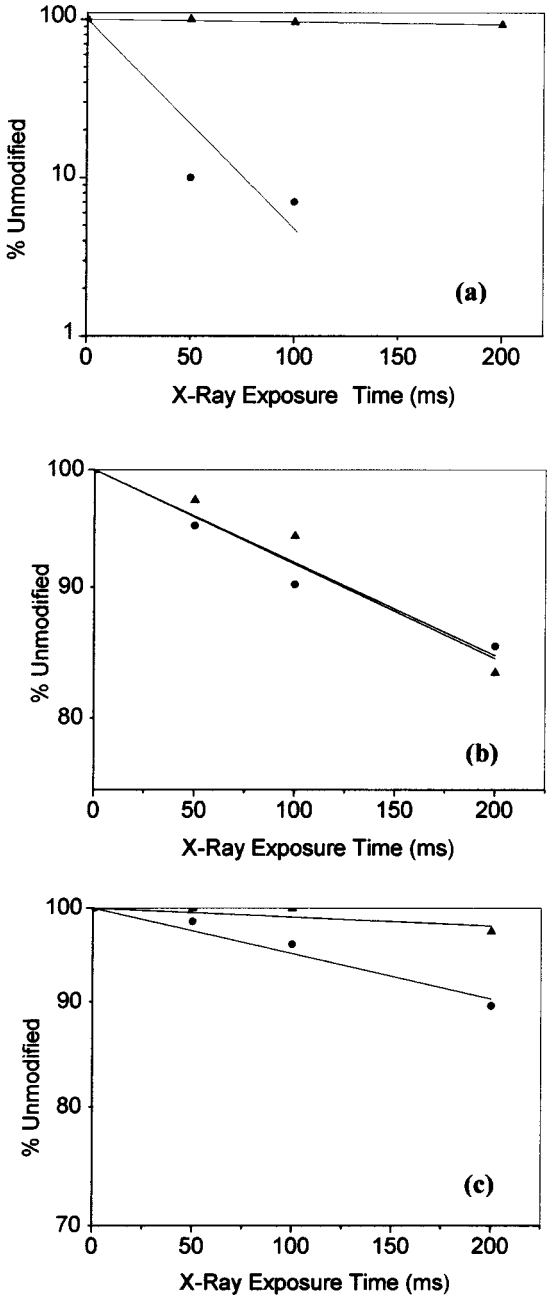

FIGURE 4: Representative dose−response curves for cofilin peptides. (a) Peptide 91−105 of cofilin in the absence (●) and presence (▲) of G-actin. (b) Peptide 123−129 of cofilin in the absence (●) and presence (▲) of G-actin. (c) Peptide 83−96 of cofilin in the absence (●) and presence (▲) of G-actin.

Protection of the Cofilin Peptides. As the reactivity of a particular residue is related to solvent accessibility, a side chain positioned at the interface of a protein−protein complex will exhibit a decreased rate of modification due to the decreased accessibility in the complex. The reactive residues and their modification rates in the absence or presence of actin are listed in Table 1. The modified or most likely to be modified amino acids in each peptide were identified by MS/MS sequencing (see below). Since the modification rates of residues 91−105 and 83−96 decreased while that of residues 123−129 remained unchanged upon G-actin binding (as shown in Figure 4), we presume residues within peptides 91−105 and 83−96 are part of the interface of the cofilin−G-actin complex while the modifiable residues

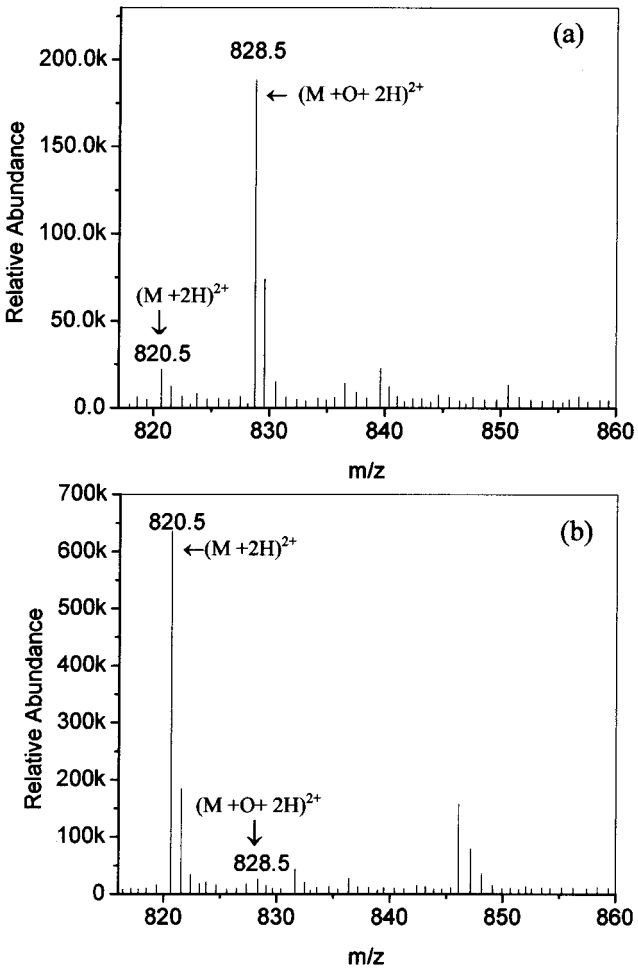

FIGURE 5: ESI-MS spectra for peptide 91−105 of cofilin (a) in the absence of G-actin and (b) in the presence of G-actin. The exposure time for these experiments is 50 ms. The unmodified ion appears at *m*/*z* 820.5, while the modified ion appears at *m*/*z* 828.5.

within peptide 123−129 are not. Digestion of the radiolyzed actin−cofilin complex produced a mixture of peptides from both actin and cofilin, which can be differentiated and unambiguously assigned by mass spectrometry. In addition to peptides 83−96, 91−105, and 123−129, eight other peptides of cofilin were obtained and identified after digestion with the proteases trypsin and Asp-N. Among the 11 peptides of cofilin that are observed to be modified and are monitored in our analysis, cofilin peptides 4−20, 10−17, 83−96, 91−105, and 106−117 exhibited a significant decrease in the rate of modification after binding to G-actin.

The quantitation of modification extent and the protection of peptide 91−105 in the actin−cofilin complex are illustrated in the MS analysis of panels a and b of Figure 5. Panel a illustrates the abundance of the modified and unmodified ions for this peptide in the case of isolated cofilin. The singly modified peptide was detected as a doubly charged ion at *m*/*z* 828.5, while the unmodified species appeared as a doubly charged ion at *m*/*z* 820.5. Comparison of the relative abundance of the peaks for modified and unmodified peptide 91−105 gave a modification extent of 90% in the absence of G-actin, while in the cofilin−actin complex, the extent of oxidation for the peptide decreased to 3% (Figure 5b). Analyzing the dose−response curves for other peptides demonstrated that significant protection occurred also on peptides 4−20, 10−17, and 106−117. Note that the modification rate results for peptide 4−20 for both isolated cofilin and the complex are identical within the error to that for peptide 10−17, and that in both cases Leu 13 was independently identified as the modifiable residue (see below). Thus, despite an entirely different proteolytic digestion and quantitation, the data are in full agreement for the change in reactivity of this side chain residue when the complex is formed. There is also overlap in the data between peptide 91−105 and peptide 83−96, as in both cases Pro 94 is the modifiable residue that is protected in the complex.

Unprotected Peptides of Cofilin. We also were able to quantitate the dose responses for six other peptides that had significant modification, but were unaffected by complex formation. These provide an important control for this methodology. In the examination of the gelsolin segment 1−actin complex, we identified two peptides whose modification rates were not changed upon complex formation (*45*). Solvent accessibility calculations for the complex indicated that the reactive residues within these peptides were not protected upon complex formation, so a change in rate was not anticipated. However, nonspecific protections arising from a general suppression of radiolysis due to more total moles of protein in solution cannot be ruled out without direct evidence. For the six peptides in question (27−36, 43−56, 18−33, 51−60, 123−129, and 130−143), the modification rates for the complex are, in every case, observed to be equal to or less than the modification rates observed for isolated cofilin. However, these decreases average only 8.5% (ranging from 0 to 23%), and in no case are the decreases greater than the respective measurement errors implied by the standard deviations of the measured rates. Thus, although there is likely to be a small amount of nonspecific protection in these experiments, it is on the order of magnitude of other experimental errors. For the five peptides where a significant change in modification rate is occurring, the decrease in the rate in the complex compared to that of isolated cofilin ranges from 63 to 99% (with an average decrease in rate of 80%). Thus, the protections observed for these five peptides are quite specific and extensive in nature and represent significant effects.

Footprinting by MALDI. To further confirm that the protections in our footprinting work are correct, we monitored the modification of peptide 83−96 for isolated cofilin and the complex by using MALDI-TOF mass spectrometry. In the absence of G-actin, the MALDI-TOF MS spectrum of peptide 83−96 exhibits an unmodified peak at *m*/*z* 1636.80 and modified peaks at *m*/*z* 1650.70, 1652.88, 1668.69, and 1684.73 corresponding to +14, +16, +32, and +48 ions, respectively. The observation of the +14 species is distinctive for proline, which has +14 and +16 oxidation products (*35*). The presence of the +32 and +48 species indicates that other side chains (likely, Phe 85, Phe 86, or Trp 88) are also modified (Figure 6a). After G-actin binding takes place, the modified peaks do not appear in the spectrum (Figure 6b), dramatically illustrating the protection from oxidation that occurs upon complex formation for this peptide.

Identification of Oxidation Site(s) by Tandem Mass Spectrometry (MS/MS). Although the data on the rates of modification indicate changes in solvent accessibility upon complex formation, modification rates do not provide any information about the specific residues that are oxidized. In

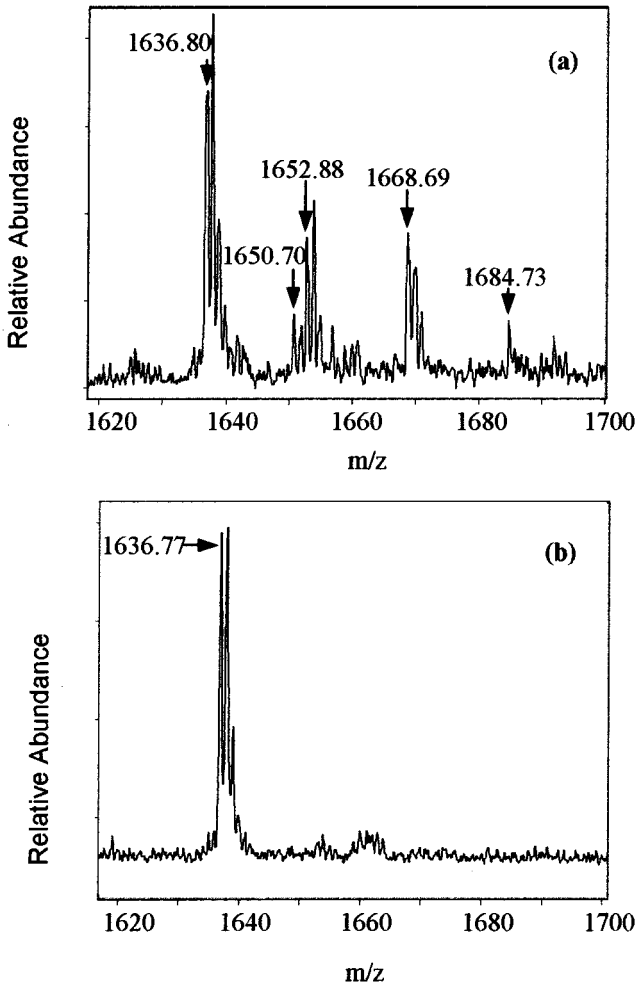

FIGURE 6: Illustration of the specific protection of cofilin peptide 83−96 upon G-actin binding using MALDI-TOF MS. (a) Cofilin exposed for 200 ms in the absence of G-actin. (b) Cofilin exposed for 200 ms in the presence of G-actin. The singly charged, unmodified peptide appears at *m*/*z* 1636−1637. In panel a, oxygen additions of one, two, and three atoms can clearly be seen. In the presence of G-actin, no modified peptide is observed.

favorable cases, MS/MS sequencing provides a direct means of identifying the site of oxidative modification (*35*−*37*, *45*). Figure 7a shows a representative collision-induced dissociation (CID) MS/MS spectrum for the peptide composed of residues 83−96 (IVFFTWSPDTAPVR). The unmodified doubly charged ion from this peptide is introduced into the collision cell, and the generated fragments are analyzed with the mass spectrometer (*41*, *42*). Daughter ions of y-type are generated when the charge is retained on the C-terminus; for example, the y_3, y_7, y_8, y_9, y_{10}, y_{11}, and y_{12} ions are clearly seen in Figure 7a. B-type ions are generated when charge is retained on the N-terminus, with b_{13}, b_{11}, b_{10}, b_9, b_7, b_6, b_5, and b_3 readily identified. Daughter ion products that fragment and ionize adequately are well-represented in the spectrum. When the same analysis is conducted on the singly oxidized, doubly charged peptide generated by radiolysis, retention of mass on a daughter ion (a shift of 16 mass units vs the ion position in Figure 7a) indicates that the daughter ion retains the site of modification. For example, in Figure 7b, the b_3, b_5, b_6, b_7, and b_{11} fragments of this peptide are not shifted at all relative to Figure 7a (b_9 and b_{10} are not observed). This suggests that oxidation takes place on the C-terminal segment PVR, and that Pro 90, Tyr 88, and Phe 85 and 86 are less likely to be oxidized, while Pro 94 is indicated since modification of valine and arginine is rarely observed. Also, Pro 94 is highly accessible (ASA = 73 Å^2), while Pro 90, Tyr 88, and Phe 86 are relatively inaccessible (Table 1). An examination of the y-series fragments indicates that for all y-series ions observed, all are shifted by +16. In fact for y_3, which includes Pro 94, no unmodified ion is observed (e.g., observation of some unmodified ion would indicate that a mixture of residues is responsible for the oxidation), supporting it as the primary target residue for this peptide. Thus, the MALDI and MS/MS sequencing data clearly show that Pro 94 is protected upon complex formation.

If oxidation occurs mainly on one residue of a peptide that contains multiple modifiable residues, the abundance of this modified residue will be far above those of the others that share the same *m*/*z* value. For example, Leu 13 in peptide 4−20, Leu 32 in peptide 27−36, Leu 13 in peptide 10−17, Leu 21 in peptide 18−33, and Phe 124 in peptide 123−129 were also identified as being exclusively oxidized by MS/MS sequencing. However, if the oxidation sites are distributed among several modifiable residues in a peptide sequence, tandem MS can identify all the residues contributing to the modification, if the ion ionizes and fragments well (e.g., sufficient signal to noise in the MS/MS spectrum is obtained). However, when the modification is distributed over several residues, and a good fragmentation pattern is not obtained, precisely locating the participating residues can be difficult. This is exactly the case for the residues comprising peptide 51−60, which did not in any case exhibit protection. Besides 51−60, other peptides (including 43−56, 91−105, and 130−143) have distributed oxidation products; however, in some cases, we can definitely assign the multiple residues involved (Table 1).

Peptide 106−117 exhibited minimal modification because of the near-zero accessibility of modifiable amino acids. Furthermore, the MS/MS spectrum of peptide 130−143 was not interpretable. Thus, we cannot unambiguously identify the modified residues by MS analysis. However, on the basis of previous work on peptides and proteins (*35*−*38*), the modification would be predicted to occur at Leu 108 and Leu 112 for peptide 106−117 and at Leu 133 and His 143 for peptide 130−143. Although Leu 108 and Leu 112 in peptide 106−117 have a low modification rate (0.1 s^{-1}), after binding to G-actin takes place, this rate decreased to essentially zero, Thus, both must be protected in the complex. For peptide 130−143, Leu 133 is quite accessible and His 143, the C-terminal residue, is disordered and likely highly accessible. Thus, both of these residues are the presumed targets for this peptide and are indicated as not participating in the interface.

DISCUSSION

Synchrotron Protein Footprinting. Synchrotron protein footprinting employs hydroxyl radicals to probe regions of a protein that undergo changes in surface accessibility as the consequence of forming a macromolecular complex and/or conformational reorganization (*35*, *38*, *45*, *51*). This technique provides detailed structural information by directly identifying the amino acid side chains that contribute to binding interfaces. In the work presented here, we described the first application of this technique in probing the interface

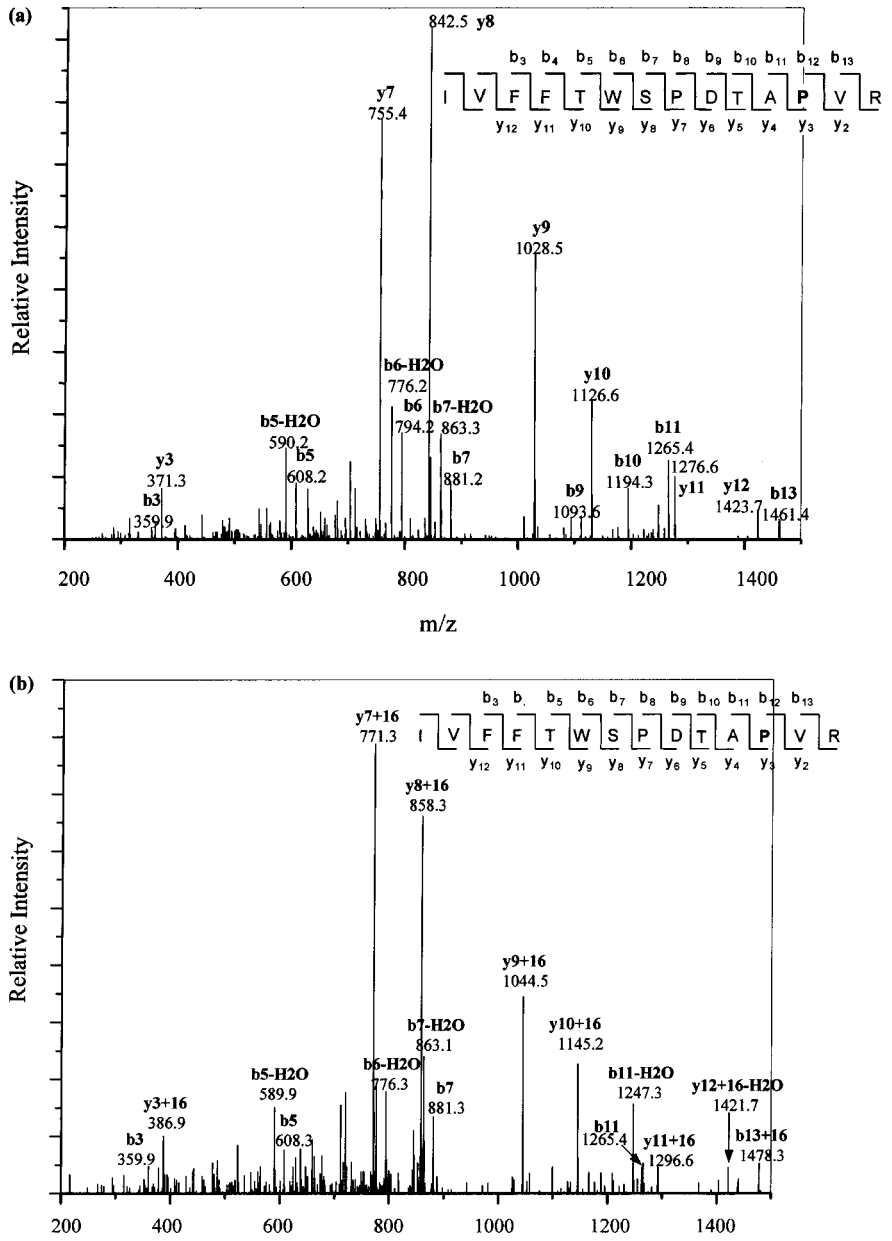

FIGURE 7: MS/MS sequencing of peptide 83−96 of cofilin. Comparison of the spectra from (a) 0 ms exposure and (b) 200 ms exposure confirms that modification occurs on Pro 94.

of a structurally uncharacterized protein complex. The presence of five peptides with significant protections and six peptides with no observed protections contributes to a detailed map of the actin binding surface of cofilin.

Several features of the footprinting methodology have been developed to ensure that the reactivity of the "native" state is monitored and that changes in reactivity due to the modifications minimally perturb the data. First, we plot the loss of *unmodified* material for a particular peptide. By contrast, analyzing the rate of formation of modified product would be much more problematic. Second, the analysis of the dose−response curves shows a constant rate of modification. If the structure were altered by modification in such a way as to, for example, unfold the protein and increase accessibility, that would tend to increase the modification rate as a function of dose. In this case, the dose−response curves would be nonlinear. It could be the case that although a particular peptide is unmodified, there exists a modification elsewhere in the protein that alters the global protein structure. However, since surface residues are generally modified, polar substitutions of such residues are likely to have a minimal effect on structure. Also, we monitor many residues to ensure integrity of the protein, including buried residues that are unmodified. In the case of unfolding, these residues would become accessible. This is not observed. Third, the short dose times available with a synchrotron provide a snapshot of the molecule during the exposure, minimizing the time available for structural change due to the oxidation. In the case of the gelsolin segment 1−actin complex (*45*), where these methods were first validated for protein−protein interactions, the crystallographic structure of the complex predicted that a phenylalanine within one of the peptides that was was analyzed should be entirely protected from solvent. Protein footprinting showed that the rate of modification of this peptide was reduced nearly 40-fold in the complex compared to the reactivity in isolated

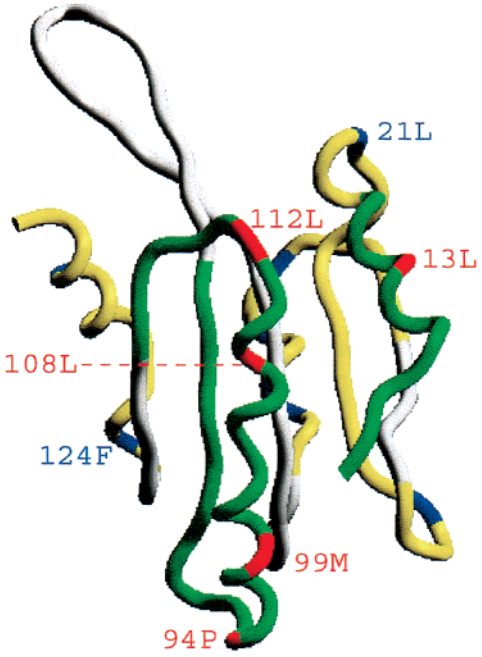

FIGURE 8: Cofilin binding surface identified by footprinting. The monitored peptides that show a modification rate decrease are colored green, and the modified side chains in these peptides are colored red. The monitored peptides that show no changes in modification rates are colored yellow, with the modified amino acids colored blue. This figure was prepared with SETOR (*55*).

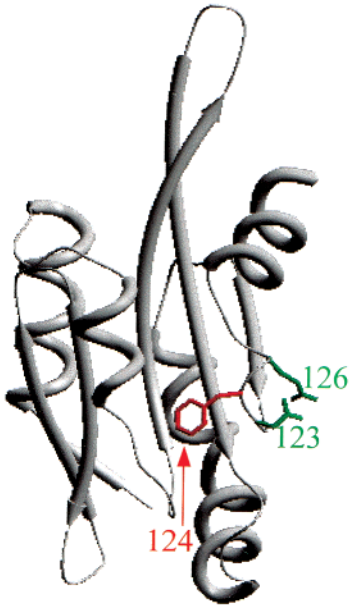

FIGURE 9: Opposite orientation of the Phe 124 side chain (red) with respect to those of Asp 123 and Glu 126 in yeast cofilin (green). While Asp 123 and Glu 126 were shown to contribute to the binding surface in the mutagenesis work (*46*), Phe 124 was not protected upon binding of cofilin and actin. Note that the orientation shown here is rotated 90° to the right from that in Figure 8. This figure was prepared with SETOR (*55*).

gelsolin segment 1. Tandem MS demonstrated that the specific phenylalanine was involved in the reaction. By comparison, peptides that were predicted to have side chains outside the interface and thus not protected upon complex formation exhibited no significant change in the rate of modification. Therefore, the use of modification rates (and dose−response curves) to measure accessibility and comparing the modification rates of peptides inside and outside of the known interface are critical to providing valid structural results. Although we emphasize in this paper the use of the technique to map an interface, we have also used footprinting to measure conformational changes of macromolecules (*36*, *38*, *51*). Complex formation in general can be accompanied by conformation changes far from the specific sites(s) of interaction. This also results in changes in reactivity, and thus, the footprinting data need to be carefully interpreted in the context of complementary approaches.

G-Actin Binding Surface of Cofilin. The cofilin residues implicated in binding actin are consistent with previously published biochemical and genetic data. Residues within peptides 4−20, 10−17, 83−96, 91−105, and 106−117 exhibit strong protection upon G-actin binding. Specifically, Leu 13, Pro 94, Met 99, and Leu 108 and 112 define a binding surface consisting of helix α3 and N-terminal segments (Figure 8). Previous mutagenesis studies have shown that Arg 96, Lys 98, and Ser 103 and 104 (corresponding to residues 119 and 120 from porcine cofilin) (*28*−*31*) are important for both F- and G-actin binding. Cross-linking studies (*32*) have also implicated the N-terminal segment of destrin, a cofilin homologue, as participating in the actin binding surface. These observations are consistent with the footprinting results presented here.

In addition, our footprinting studies indicate that peptide 106−117 is protected; we suggest that this protection involves Leu 108 and 112, but due to the small extent of modification, the tandem MS data are equivocal. In addition, these residues are judged to be inaccessible by VADAR analysis. It is possible that some flexibility in this region allows transient accessibility that is eliminated upon complex formation, or that small differences in structure in solution versus the crystal exist. An important additional caveat is that besides protection by contact, induced conformational change distinct from the binding site can occur. That is, binding of actin could cause a rearrangement that buries this segment without it directly contacting actin. These experiments cannot directly distinguish these two possibilities. Nonetheless, the contribution from peptide 106−117 to the actin binding site is consistent with recent work (*56*), in which mutations of R109 to A and R110 to A were shown to reduce the extent of G-actin binding.

Although the N-terminal region of cofilin has been suggested to be essential for both G- and F-actin binding, including residues 1−4 (*28*), the exact binding sites in helix α1 have been unclear. We show here that the binding surface extends to Leu 13 as seen in the protection of peptides 4−20 and 10−17, but does not include Leu 21 since peptide 18−33 shows no protection. In addition, the X-ray footprinting results suggest that the entire cofilin α3 segment contributes to the actin binding surface. Furthermore, the data suggest the binding surface extends to Pro 94, which is one residue prior to the start of helix α3. This residue was well-protected from hydroxyl radical modification in the presence of actin. This is significant, as previous work has not identified any amino acid in this region that is important for actin binding. Mutagenesis studies have suggested that Asp 123 and Glu 126 in the loop between β6 and α4 were essential for both G- and F-actin binding (*28*). Surprisingly, our footprinting of peptide 123−129 shows that no protection occurred on Phe 124 in this loop, suggesting that Phe 124 in this loop

does not contribute to the binding site. However, these results are not necessarily inconsistent, since the mutagenesis experiments were limited to examination of the charged residues, whereas the footprinting approach probed only the aromatic residues within this region. In fact, as can be seen in Figure 9, the side chain of Phe 124, compared to those of Asp 123 and Glu 126, is oriented in opposite directions such that Phe 124 is pointed away from the observed actin binding face of cofilin. Thus, the footprinting and mutagenesis results are consistently explained by the proposed actin binding interface of cofilin, and the techniques are fully complementary.

CONCLUSIONS

We have used synchrotron protein footprinting to identify yeast cofilin residues that contribute to the G-actin binding surface. This surface includes Pro 94 just prior to helix α3, the long α3 helix (residues M99, L108, and L112), and the N-terminal segments that encompass Leu 13. In contrast, a number of modified residues, such as Leu 21, Phe 124, Leu 133, and His 143, are not protected and thus are not predicted to participate in the binding interface, and in conclusion, these observations provide a more comprehensive view of the cofilin−actin interface.

ACKNOWLEDGMENT

We are grateful to Dr. Fang Wang for her technical assistance with the facilities in the Laboratory for Macromolecular Analysis and Proteomics of the Albert Einstein College of Medicine.

REFERENCES

1. Bassell, G., and Singer, R. H. (1997) *Curr. Opin. Cell Biol. 9*, 105−115.
2. Condeelis, J. (1997) *Trends Cell Biol. 20*, 169−171.
3. Fishkind, D. J., and Wang, Y. L. (1995) *Curr. Opin. Cell Biol. 7*, 23−31.
4. Pollark, R., Osborn, M., and Weber, K. (1975) *Proc. Natl. Acad. Sci. U.S.A. 93*, 10703−10706.
5. Pollard, T. D. (1990) *Curr. Opin. Cell Biol. 2*, 33−40.
6. Weeds, A. (1982) *Nature 296*, 811−816.
7. Cramer, L. P., Mitchison, T. J., and Theriot, J. A. (1994) *Curr. Opin. Cell Biol. 6*, 82−86.
8. Ben-Ze'ev, A. (1997) *Curr. Opin. Cell Biol. 9*, 99−108.
9. Moon, A., and Drubin, D. G. (1995) *Mol. Biol. Cell 6*, 1423−1431.
10. Bamburg, J. R. (1999) *Annu. Rev. Cell Dev. Biol. 15*, 185−230.
11. Bamburg, J. R., McGough, A., and Ono, S. (1999) *Trends Cell Biol. 9*, 364−370.
12. Southwick, F. S. (2000) *Proc. Natl. Acad. Sci. U.S.A. 97*, 6936−6938.
13. Hawkins, M., Pope, B., Maciver, S. K., and Weeds, A. G. (1993) *Biochemistry 32*, 9985−9993.
14. Hayden, S. M., Miller, P. S., Brauweiler, A., and Bamburg, J. R. (1993) *Biochemistry 32*, 9994−10004.
15. Condeelis, J. (2001) *Trends Cell Biol. 11*, 288−293.
16. Du, J., and Freiden, C. (1998) *Biochemistry 37*, 13276−13284.
17. Maciver, S. K., Pope, B. J., Whytock, S., and Weeds, A. G. (1998) *Eur. J. Biochem. 256*, 388−397.
18. Ichetovkin, I., Han, J. H., Pang, K. M., Knecht, D. A., and Condeelis, J. S. (2000) *Cell Motil. Cytoskeleton 45*, 293−306.
19. Carlier, M. F., Laurent, V., Santolini, J., Melki, R., Didry, D., Xia, G. X., Hong, Y., Chua, N. H., and Pantaloni, D. (1997) *J. Cell Biol. 136*, 1307−1323.
20. Pope, B. J., Gonsior, S. M., Yeoh, S., McGough, A., and Weeds, A. G. (2000) *J. Mol. Biol. 298*, 649−661.
21. Angnew, B. J., Minamide, L. S., and Bamburg, J. R. (1995) *J. Biol. Chem. 270*, 17582−17587.
22. Arber, S., Barbayannis, F. A., Hanser, H., Schneider, C., Stanyon, C. A., Bernard, O., and Caroni, P. (1998) *Nature 393*, 805−809.
23. Yang, N., Higuchi, O., Ohashi, K., Nagata, K., Wada, A., Kangawa, K., Nishida, E., and Mizuno, K. (1998) *Nature 393*, 809−812.
24. Yonezawa, N., Nishida, E., Lida, K., Yahara, I., and Sakai, H. (1990) *J. Biol. Chem. 265*, 8382−8386.
25. Rozycki, M. D., Myslik, J. C., Shutt, C. E., and Lindberg, U. (1994) *Curr. Opin. Struct. Biol. 6*, 87−95.
26. McGough, A., Pope, B., Chiu, W., and Weeds, A. (1997) *J. Cell Biol. 138*, 771−781.
27. Galkin, V. E., Orlova, A., Lukoyanova, N., Wriggers, W., and Egelman, E. H. (2001) *J. Cell Biol. 153*, 75−86.
28. Lappalainen, P., Fedorov, E. V., Fedorov, A. A., Almo, S. C., and Drubin, D. G. (1997) *EMBO J. 16*, 5520−5530.
29. Moriyama, K., Yonezawa, N., Sakai, H., Yahara, I., and Nishida, E. (1992) *J. Biol. Chem. 267*, 7240−7244.
30. Moriyama, K., and Yahara, I. (1999) *EMBO J. 18*, 6752−6761.
31. Ono, S., McGough, A., Pope, B. J., Tolbert, V. T., Bui, A., Pohl, J., Benian, G. M., Gernert, K., and Weeds, A. G. (2001) *J. Biol. Chem. 276*, 5952−5958.
32. Sutoh, K., and Mabuchi, I. (1989) *Biochemistry 28*, 102−106.
33. Hatanaka, H., Ogura, K., Moriyama, K., Ichikawa, S., Yahara, I., and Inagaki, F. (1996) *Cell 85*, 1047−1055.
34. Wriggers, W., Tang, J. X., Azuma, T., Marks, P. W., and Janmey, P. A. (1998) *J. Mol. Biol. 282*, 921−932.
35. Maleknia, S. M., Brenowitz, M., and Chance, M. R. (1999) *Anal. Chem. 71*, 3965−3973.
36. Maleknia, S. M., Ralston, C. Y., Brenowitz, M. D., Doward, K. M., and Chance, M. R. (2001) *Anal. Biochem. 289*, 103−115.
37. Kiselar, J. G., Maleknia, S. D., Sullivan, M., Chance, M. R., and Downard, K. M. (2002) *Int. J. Radiat. Biol. 78*, 101−114.
38. Chance, M. R. (2001) *Biochem. Biophys. Res. Commun. 287*, 614−621.
39. Garrison, W. M. (1987) *Chem. Rev. 87*, 381−389.
40. Klassen, N. V. (1987) in *Radiation chemistry: principles and applications* (Farhataziz and Rodgers, M. A. J., Eds.) pp 29−61, VCH, New York.
41. Roepstorff, P., and Fohlmann, J. (1984) *J. Biomed. Mass Spectrosc. 11*, 601.
42. Biemann, K. (1988) *Biomed. Environ. Mass Spectrosc. 16*, 99−111.
43. Dharmasiri, K., and Smith, D. L. (1996) *Anal. Chem. 68*, 2340−2344.
44. Deng, Y., Pan, H., and Smith, D. L. (1999) *J. Am. Chem. Soc. 121*, 1966−1967.
45. Goldsmith, S. G., Guan, J.-Q., Almo, S. C., and Chance, M. R. (2001) *J. Biomol. Struct. Dyn. 19*, 405−419.
46. Fedorov, A. A., Lappalainen, P., Fedorov, E. V., Drubin, D. G., and Almo, S. C. (1997) *Nat. Struct. Biol. 4*, 366−369.
47. Kabsch, W., Mannherz, H. G., Suck, D., Pai, E. F., and Holmes, K. C. (1990) *Nature 347*, 37−44.
48. Otterbein, L., Graceffa, P., and Dominguez, R. (2001) *Science 293*, 708−711.
49. Spudich, J. A., and Watt, S. (1971) *J. Biol. Chem. 246*, 4866−4871.
50. Richard, F. M. (1974) *J. Mol. Biol. 82*, 1−14.
51. Sclavi, B., Woodson, S. A., Sullivan, M., Chance, M. R., and Brenowitz, M. (1998) *Methods Enzymol. 295*, 379−402.
52. Nishida, E., Maekawa, S., and Sakai, H. (1984) *Biochemistry 23*, 5307−5313.
53. Nishida, E. (1985) *Biochemistry 24*, 1160−1164.
54. McLaughlin, P. J., Gooch, J. T., Mannherz, H. G., and Weeds, A. G. (1993) *Nature 364*, 685−692.
55. Evans, S. V. (1993) *J. Mol. Graphics 11*, 134−138.
56. Ojala, P. J., Paavilainen, V., and Lappalainen, P. (2001) *Biochemistry 40*, 15562−15569.
57. Richmond, T. J. (1984) *J. Mol. Biol. 178*, 63−89.

BI0121104